Microbridge structures for uniform interval control of flowing droplets in microfluidic networks

Do-Hyun Lee,[1] Wonhye Lee,[1] Eujin Um,[1] and Je-Kyun Park[1,2,a)]
[1]*Department of Bio and Brain Engineering, College of Life Science and Bioengineering, Korea Advanced Institute of Science and Technology (KAIST), 291 Daehak-ro, Yuseong-gu, Daejeon 305-701, Republic of Korea*
[2]*KAIST Institute for the NanoCentury, 291 Daehak-ro, Yuseong-gu, Daejeon 305-701, Republic of Korea*

(Received 30 May 2011; accepted 26 July 2011; published online 16 August 2011)

Precise temporal control of microfluidic droplets such as synchronization and combinatorial pairing of droplets is required to achieve a variety range of chemical and biochemical reactions inside microfluidic networks. Here, we present a facile and robust microfluidic platform enabling uniform interval control of flowing droplets for the precise temporal synchronization and pairing of picoliter droplets with a reagent. By incorporating microbridge structures interconnecting the droplet-carrying channel and the flow control channel, a fluidic pressure drop was derived between the two fluidic channels *via* the microbridge structures, reordering flowing droplets with a defined uniform interval. Through the adjustment of the control oil flow rate, the droplet intervals were flexibly and precisely adjustable. With this mechanism of droplet spacing, the gelation of the alginate droplets as well as control of the droplet interval was simultaneously achieved by additional control oil flow including calcified oleic acid. In addition, by parallel linking identical microfluidic modules with distinct sample inlet, controlled synchronization and pairing of two distinct droplets were demonstrated. This method is applicable to facilitate and develop many droplet-based microfluidic applications, including biological assay, combinatorial synthesis, and high-throughput screening. © *2011 American Institute of Physics*. [doi:10.1063/1.3625604]

I. INTRODUCTION

The advancement of droplet-based microfluidics has attracted much attention in recent years because of its utility in isolating specific cells individually within nano- to femto-liter droplets[1] and manipulating them in microfluidic devices for achieving various chemical reactions.[2] In addition, microdroplets have great potential applications for high-throughput biochemical synthesis[3] and screening[4] based on the accurate droplet fusion and mixing controls. Possible cross-contamination between droplets can be eliminated by precise control in time and space,[5] resulting in perfect compartmentalized vessels to reduce experimental errors. Until now, various droplet-based microfluidic platforms have already been applied for several applications such as protein–protein interaction,[6] polymerase chain reaction,[7] cell-based enzymatic assay,[8,9] directed evolution,[10] and nanoparticle synthesis[11] to puzzle out biological and chemical problems.

To achieve a variety range of chemical and biochemical reactions, precise combination of droplets containing distinct reagents is required to control coalescence and mixing of droplets. In particular, combinatorial pairing of different droplets would be important for many multiplexed assays and polymer encapsulation techniques in microfluidic systems. Spontaneous and combinatorial pairing of droplets requires precise synchronization of approaching droplets in time and space by adjusting the droplet interval. However, in order to prevent irregularities in the spacing control of droplets, it is required to integrate with additional microfluidic components such as electrode for

[a)]Electronic mail: jekyun@kaist.ac.kr. Tel: +82-42-350-4315. Fax: +82-42-350-4310.

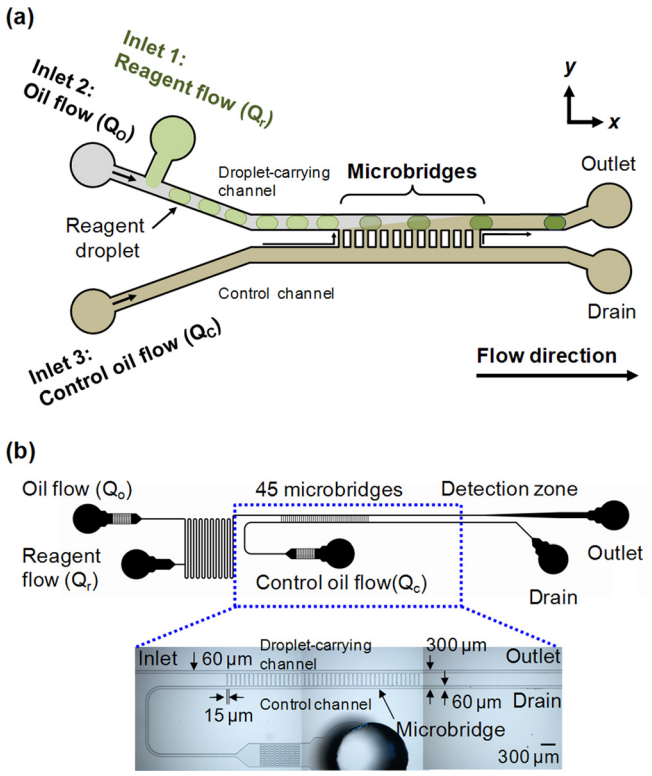

FIG. 1. (a) A schematic of the microfluidic device integrated with microbridge structures interconnecting droplet-carrying and control channels. Two inlets of the droplet-carrying channel (inlets 1 and 2) are for introduction of reagent (Q_r) and oil flow (Q_o), and the inlet of the control channel (inlet 3) is for introduction of control oil flow (Q_c). A fluidic pressure drop between two channels *via* 45 microbridges can be used to adjust the interval at the droplet-carrying channel, enabling the flexible and precise temporal control of droplets. (b) Channel design of the microfluidic device and enlarged view of fabricated microbridge structures. All fluidic channel and microbridge structures were fabricated from PDMS using standard soft lithographic methods. The overall thickness of the channel was designed to be 35 μm.

applying electric field[12,13] or multi-layered chambers[14] and valves[15] for temporal stopping droplets. These integration issues have limitations in further incorporation of other microfluidic components for extra droplet manipulation. In addition, passive hydrodynamic coupling at two opposing nozzles to produce droplet pairs was demonstrated,[11,16] but flexible control of pairing aspects is not available under the constant patterns of droplet-generating states and size of droplets.

To address the above needs, we suggest a facile and robust microfluidic control module which is integrated with simple microbridge structures[17] connected to additional inlets for adjusting the interval between two approaching microdroplets. Temporal control of droplets is achieved by the flow rate in a control channel, without complicated control of droplet-carrying flow rates, any additional microfluidic components and external forces. By adjusting the flow rate of control oil flow as bias, the droplet interval is dynamically altered when droplet-carrying flow rates are constant [Fig. 1(a)]. We also demonstrate the robustness of the temporal spacing method for practical applications of alginate droplets by introducing the oil phase including calcium chloride as a control flow. Based on the difference of control oil flow rate, alginate droplets containing live cells are rapidly solidified and efficiently collected at the outlet with suitable droplet spacing. Moreover, controlled pairing of droplets is demonstrated by temporal synchronization of generated droplet pairs.

II. MATERIALS AND METHODS

A. Materials

Sodium alginate (A0682-100G, Sigma) was dissolved in distilled water by 1% (w/w) and filtered with a 0.22-μm syringe filter (Millex-GV, Millipore) to remove any clumps of alginate.

Solutions of orange food dye (Kemide Co., Jeonju, Korea) were mixed with alginate solution to visualize droplets. Oleic acid without any surfactant was introduced as a continuous phase and the alginate was gelated by the oleic acid (Sigma) with calcium. 0.6 g of calcium chloride (C7902-500G, Sigma) was dissolved in 25 ml of oleic acid *via* ultrasonication. Due to the low solubility of calcium chloride and oleic acid, calcium chloride was dissolved in 25 ml of 2-methyl-1-propanol (J.T. Baker, Deventer, The Netherlands) *via* ultrasonication. After mixing of the calcium chloride and oleic acid at a ratio of 50% (v/v), the 2-methyl-1-propanol was distilled in a convection oven at 65 °C for a day.

U937 cell line (human leukemic monocyte lymphoma cell line) was cultured in RPMI 1640 medium (Invitrogen, CA) supplemented with 10% (v/v) heat-inactivated fetal bovine serum (Invitrogen), 100 units/ml penicillin G and 100 μg/ml streptomycin. The cell cultures were maintained in a humidified atmosphere containing 5% CO_2. Then cells were centrifuged at 1000 rpm for 3 min for removing supernatant and stained with 10 μm CellTracker Green CMFDA (Molecular Probes Inc., Eugene, OR).

B. Design and fabrication of a microfluidic device

A microfluidic device was fabricated by using a conventional poly(dimethylsiloxane) (PDMS) (Sylgard 184; Dow Corning, Midland, MI) molding process. The elastomer was mixed with a curing agent in a ratio of 10:1 (w/w). The negative photoresist SU-8 2025 (MicroChem Corp., Newton, MA) on a silicon wafer was used for a PDMS mold. PDMS was cast on the mold and cured for 3 h in a convection oven at 65 °C for complete cross-linking. The PDMS channel was irreversibly sealed with a glass slide after exposure to oxygen plasma for 30 s. Because the hydrophobic PDMS microchannel became hydrophilic during plasma treatment, the device was stored in a convection oven at 65 °C for 2 days to recover hydrophobic nature of the microchannel. After the fabrication process, the microfluidic devices were sterilized with 6% (w/v) Pluronic F127 in distilled water prior to cell loading without mammalian cell attachment. Subsequently, the microchannels were flushed with an oleic acid.

We prepared liquid droplets in mineral oil mixed with 0.5% (w/w) Span 80 (Sorbitan monooleate, Sigma–Aldrich Co.) by hydrodynamic flow focusing at the T-junction where each stream of oil and liquid is came from two different injection channels. The entire dimension of the device as shown in Fig. 1(b) was about 33 mm $\times$ 6 mm. The widths of the aqueous and oil channels were 40 and 60 μm, respectively. The width and length of the microbridge were 15 and 300 μm, respectively. The width of outlet detection region for measuring the spacing of gelated alginate droplets was 300 μm. The height of the channel was 35 μm. The diverging microchannel of detection zone nearby the outlet plays a role in the velocity reduction of the gelated alginate beads and thus the U937 cells inside the beads would be easily observed in the microscope.

C. Experimental setup

The droplet movements were recorded by a charge-coupled detector (CCD) camera (DS-U1; Nikon Instruments Inc., Melville, NY). A commercial image analyzing program, i-Solution (IMT i-solution Inc., Korea) was used to measure the interval of droplets. All fluids were injected and motivated *via* the syringe pumps (Pump 11 Pico Plus; Harvard Apparatus, Inc., Holliston, MA) at a range of volumetric flow rates.

III. RESULTS AND DISCUSSION

Figure 1(a) illustrates a schematic diagram of the droplet interval control module integrated with microbridge structures interconnecting droplet-carrying and control channels. By incorporating microbridge structures bridging two microchannels, a pressure drop through 45 microbridges can be used to adjust the interval at the droplet-carrying channel. First, droplets are generated at the T-junction[18] in the droplet generating channel (see inlets 1 and 2), and then conveyed to the temporal control region which is connected to the microbridge structures. The control oil flow is introduced to the control channel with additional inlet (see inlet 3) and

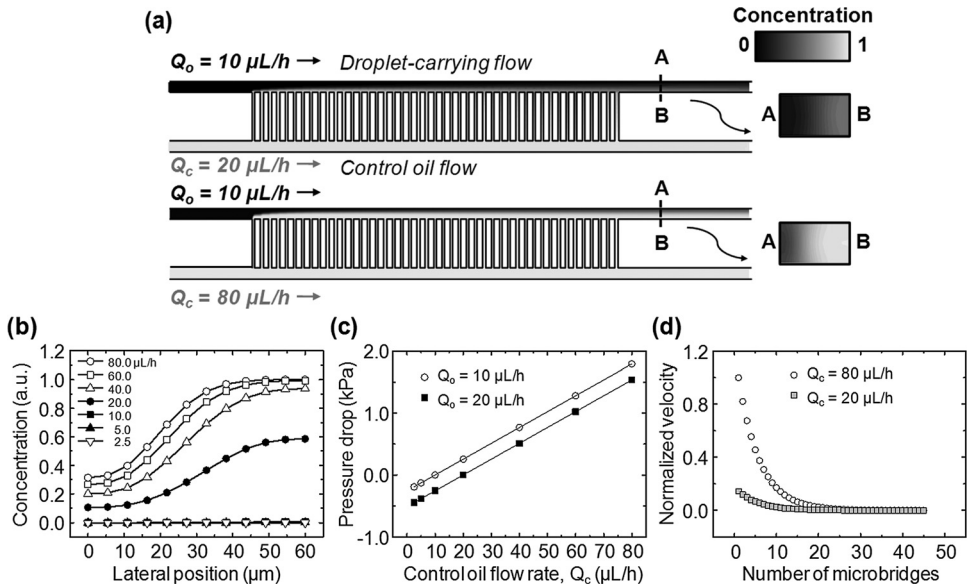

FIG. 2. (a) Simulation results of flow characteristics with an increase of the additional flow from the control channel. The cross-sectional images acquired nearby outlet show the concentration distributions of two different flows at a control oil flow rate (Q_c) of 20 and 80 μl/h, respectively, maintaining a constant oil flow rate (Q_o) of 10 μl/h. An additional oil flow field causes the migration of control oil flow passing through each microbridge due to a fluidic pressure drop between two channels, thereby enhancing the velocity of the droplet-carrying flow and inducing the temporal spacing of droplets. (b) Plot of the concentration distributions along the line from A to B in panel a as the flow rate in the control channel (Q_c) increases from 2.5 to 80 μl/h. (c) Plot of the calculated pressure drop between two channels according to the control oil flow rate (Q_c) at two different oil flow rate (Q_o). (d) Plot of the calculated normalized velocity distribution through the microbridges according to the microbridge number. Each data point represents the *y*-axial velocity in the center of each microbridge at the two different control oil flow rate (Q_c).

changes the velocity of the droplet-carrying flow *via* the microbridge structures. The long and narrow microbridge structures play a role in maintaining the shape and size of droplets, and changing the interval of neighboring droplets quickly.

To figure out the flow characteristics along the microbridge by the control oil flow, we calculated the concentration changes by two flows for different flow rate in the control channel of 20 and 80 μl/h with a fixed flow rate of 10 μl/h in the droplet-carrying channel using a commercial CFD solver (CFD-ACE+; ESI-CFD Inc., Huntsville, AL) [Fig. 2(a)]. The insets are the enlarged views of the concentration distribution by the change in the control oil flow rate (Q_c). The augmented migration of additional flow passing through each microbridge from the control channel appeared as the control oil flow rate increased. Also, we plotted the calculated concentration distributions across the lateral position of microchannel at the outlet of droplet-carrying channel as the control oil flow rate increases [Fig. 2(b)]. The relatively high input pressure field from the control oil flow generates pressure difference between two flows across the microbridge and thus gives it a chance to increase the droplet interval. The simulated tendency of pressure drop between two microchannels at the first microbridge structure for different flow rate in the droplet-carrying channel of 10 and 20 μl/h was plotted as the control oil flow rate increases [Fig. 2(c)]. We also calculated and plotted the normalized velocity distribution through the microbridges according to the microbridge number [Fig. 2(d)]. The *y*-axial velocity at the center of each microbridge decreases more steeply under the higher flow rate condition of the control channel. This means that the number of microbridge structures is enough for shifting of the control oil flow toward the droplet-carrying channel at the various flow rate conditions. Modulating the number of microbridge structures would be necessary to achieve the temporal spacing at the wide or narrow range of the control flow rate.

We could predict that the spacing between droplets would be regarded as a function of the control oil flow rate. The negative pressure drop would decelerate a train of droplets. Therefore,

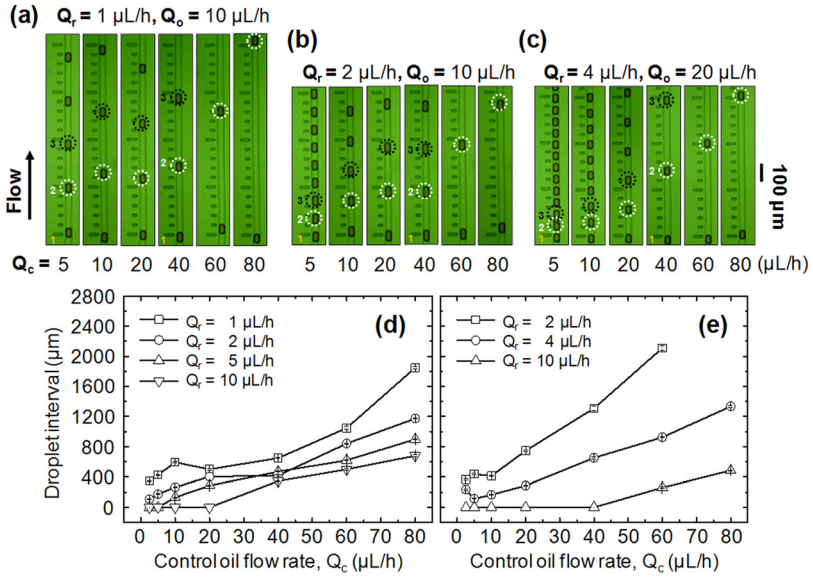

FIG. 3. Droplet interval control with respect to the control oil flow rate (Q_c) in the control channel. Microscopic images of varying droplet interval within droplet-carrying channel with respect to the flow rate in the control channel at the fixed flow rates of aqueous (Q_r) and oil phase (Q_o) (a) 1 and 10 μl/h, (b) 2 and 10 μl/h, and (c) 4 and 20 μl/h, respectively. White and black dashed circles follow 2nd and 3rd droplet of the train of droplets which was temporally controlled by control oil flow, respectively. Plot of the droplet interval with respect to the control oil flow rate (Q_c) and reagent flow rate (Q_r) at the condition of droplet generation with an oil flow rate (Q_o) of (d) 10 and (e) 20 μl/h.

the droplet interval in the droplet-carrying channel was flexibly and precisely tuned by controlling the flow rate in the control channel at a fixed flow rate in the droplet-carrying channel.

Figures 3(a)–3(c) show the microscopic images of varying droplet interval within droplet-carrying channel with respect to the flow rate in the control channel (Q_c) from 5 to 80 μl/h. The fixed flow rates of aqueous (Q_r) and oil phase (Q_o) in each trial were 1 and 10 μl/h [Fig. 3(a)]; 2 and 10 μl/h [Fig. 3(b)]; 4 and 20 μl/h [Fig. 3(c)], respectively. The "initial" interval of droplets, which is the same with droplet generating pattern at the T-junction without any temporal control, increased as the flow rate of aqueous phase decreased. The results indicate that droplets introduced to the droplet-carrying channel were temporally controlled by the additional control oil flow along the microbridges. Therefore, the interval between two approaching droplets could be adjusted by simply changing the flow rates in the control channel without any additional operation of droplet-carrying flow. We measured the droplet interval with respect to the control oil flow rate (Q_c) at the condition of droplet generation with an oil flow rate (Q_o) of 10 and 20 μl/h [Figs. 3(d) and 3(e)]. The droplet interval was defined as the distance between two neighboring droplets which were passed through the temporal control region and located near the outlet. When the flow rate in the control channel (Q_c) was adjusted from 5 to 80 μl/h, the droplet interval was changed from 114.94 ± 4.98 to 1336 ± 14.93 μm, at the fixed condition of droplet generation with a reagent flow rate (Q_r) of 4 μl/h and oil flow rate (Q_o) of 20 μl/h ($n = 3$). The zero value of the droplet interval indicates unpredictable merging of adjacent droplets due to insufficient spacing. As shown in Figs. 3(d) and 3(e), the change of droplet interval against the control oil flow rate was relatively greater as the reagent flow rate (Q_r) became lower than 10 μl/h. In addition, the droplet interval increased as the flow rate in the control channel increased, without any effect on the droplet size or generating pattern. These droplet movements can be described based on momentum balance at the pressure-driven flow through a narrow rectangular channel of height h and length L.[19] The maximum velocity is then found from an overall momentum balance, $v_{max} = \Delta p h^2 / 8 \mu_{oil} L$, where Δp is the pressure drop; μ_{oil} is the viscosity of continuous phase. Thus, the droplet velocities can be changed by adjusting pressure difference between two channels which depends on the control oil flow rate (Q_c). The linear tendency of the predicted pressure difference as shown in Fig. 2(c) is similar to the experimental ones.

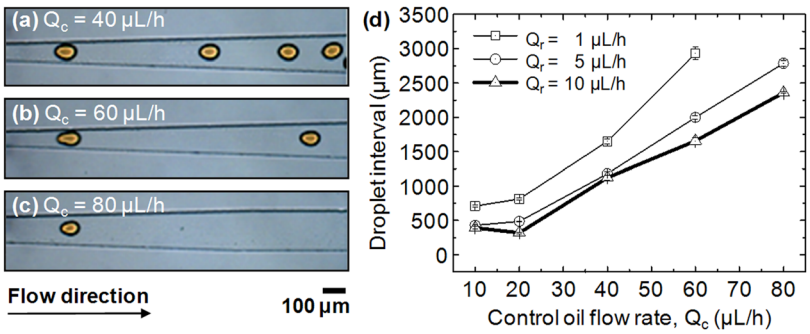

FIG. 4. Microscopic images of the gelated hydrogel beads taken at the channel outlet with respect to the control flow rate (Q_c) of (a) 40, (b) 60, and (c) 80 μl/h. (d) Plot of the droplet interval measured at the detection zone with respect to the control oil flow rate at the condition of alginate droplet generation with an oil flow rate (Q_o) of 10 μl/h, while the reagent flow (Q_r) varied from 1 to 10 μl/h. The results indicate that alginate droplets introduced to the droplet-carrying channel were temporally controlled and polymerized by the additional flow including calcified oleic acid.

For complete temporal control of droplets, it is important to maintain a stable flow throughout the microchannel. The relatively low control oil flow rate ($Q_c \leq 20$ μl/h) at the low oil flow rate ($Q_o = 10$ μl/h) may be insufficient in temporal controlling of droplets due to the small variations in flow fluctuation from the pumps. Also, insufficient spacing between adjacent droplets owing to low volumetric flow rates may influence the resistive hydrodynamic coupling effects with several droplets.[20] As shown in Fig. 3(a) and 3(b), the interval control data showed some irregular variations, resulting from an unstable microflow at the flow condition as mentioned above. This handicap at low flow rate levels can be overcome by reducing the length and increasing the number of microbridge structures for achieving sufficient droplet spacing.

For practical purpose, this microfluidic module was used for on-chip polymerization and recovery of hydrogel beads. The additional control oil flow including calcified oleic acid leads to adjust droplet interval and gelation of the alginate droplet simultaneously through the microstructures. The demonstrations of the interval control of alginate droplets were performed within microchannels integrated with microbridges. Figures 4(a)–4(c) show the enlarged images of the alginate beads gelated with calcified oleic acid taken at the channel outlet injected with different flow rates (40, 60, and 80 μl/h) in the control channel. The diameter of the alginate bead was approximately 69.6 μm. Figure 4(d) shows the plot of the measured droplet interval with respect to the control

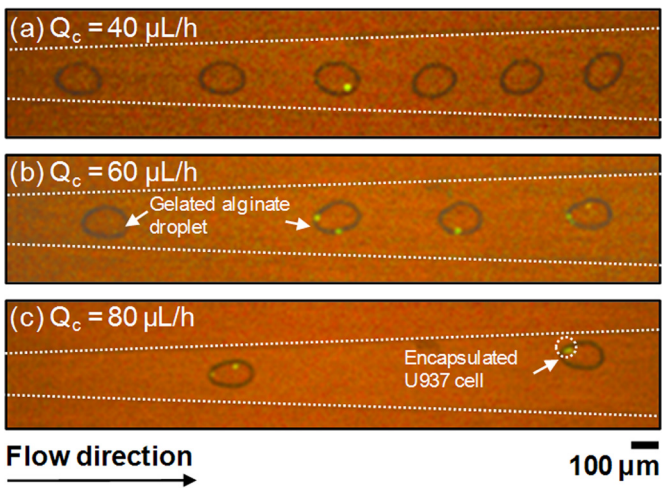

FIG. 5. Microscopic images of the cell-laden alginate beads with varying interval taken at the channel outlet with respect to the control oil flow rate (Q_c) of (a) 40, (b) 60, and (c) 80 μl/h. Dashed circles indicate the U937 cell encapsulated in the alginate bead. The fixed flow rates of alginate solution (Q_r) and oleic acid (Q_o) were 1 and 10 μl/h, respectively.

oil flow rate (Q_c). When the flow rate in the control channel was adjusted from 20 to 60 μl/h, the droplet interval was changed from 710 ± 17.32 to 2930 ± 88.88 μm, at the fixed condition of droplet generation with a reagent flow rate (Q_r) of 1 μl/h and oil flow rate (Q_o) of 10 μl/h ($n = 3$). The results indicate that alginate droplets introduced to the droplet-carrying channel were also temporally controlled and polymerized by the additional control oil flow along the microtunnels. Figure 5 shows the enlarged images of the U937 cell-laden alginate beads gelated with calcified oleic acid taken at the channel outlet injected with different flow rates (40, 60, and 80 μl/h) in the control channel. The diameter of the cell-laden alginate bead was approximately 99.8 μm. The fixed flow rates of alginate solution (Q_r) and oleic acid (Q_o) were 1 and 10 μl/h, respectively. When the flow rate of calcified oleic acid was high, the shape of polymerized alginate beads was not spherical and uniform because the calcium passage through the microbridges was increased. Also, the polymerization would be accelerated when the concentration of calcium chloride was high. The insufficient calcium passage from the control channel due to the lower control oil flow rate (lower than $Q_c = 20$ μl/h) would be lead to unexpected droplet merging in the collecting chamber because

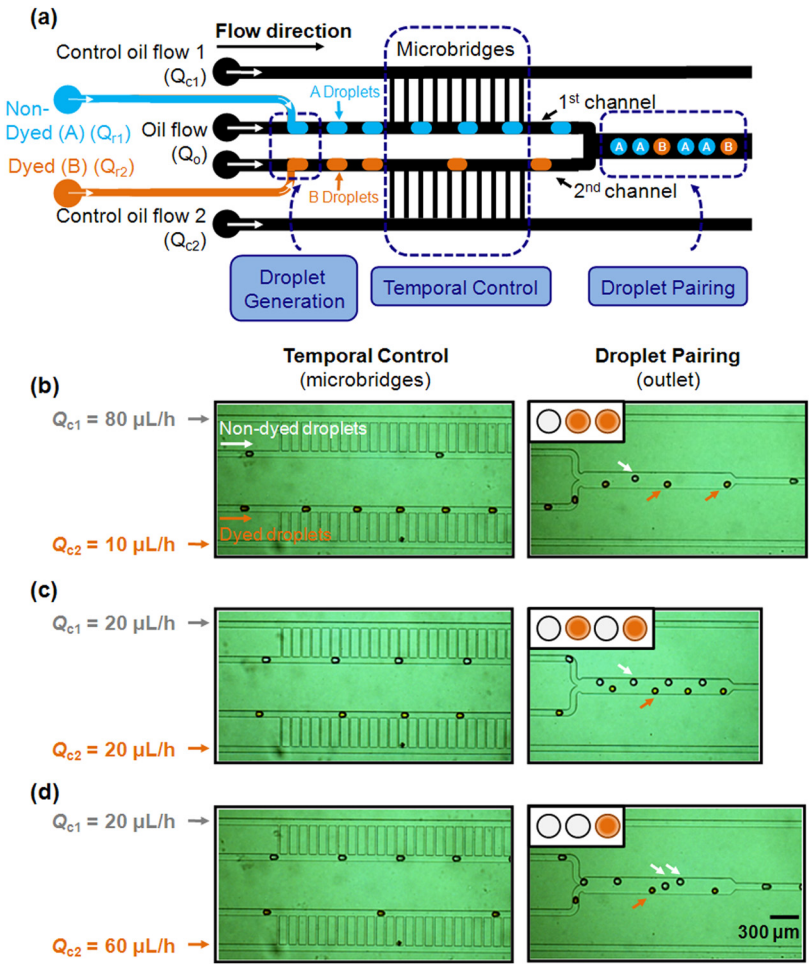

FIG. 6. Production of combinatorial droplet pairs by droplet synchronization in the microfluidic channel. (a) The layout of the parallel-linked channel for the dynamic control of droplets and the confluence channel for the production and observation of droplet pairing. Non-dyed (blue) and dyed (orange) aqueous phase was introduced to each inlet. Non-dyed and dyed droplets emerged from each T-junction were temporally controlled by changing the flow rate of each control flow (Q_{c1} and Q_{c2}). Microscopic images of the dynamic control of droplet interval at the microbridge and adjusted droplet pairing ratio (non-dyed: dyed) of (b) 1:2, (c) 1:1, and (d) 2:1 at the confluence channel when (b) $Q_{c1} = 80$ μl/h and $Q_{c2} = 10$ μl/h, (c) $Q_{c1} = 20$ μl/h and $Q_{c2} = 20$ μl/h, and (d) $Q_{c1} = 20$ μl/h and $Q_{c2} = 60$ μl/h, respectively. Each inset in (b)–(d) shows a schematic of pairing sequence in droplet pairs. White and orange arrows in each droplet pairing images indicate non-dyed and dyed droplets, respectively. All conditions of droplet generating flow were fixed as $Q_{r1} = Q_{r2} = 4$ μl/h and $Q_o = 20$ μl/h.

of weak gelation (data not shown). The encapsulated cells were located on the droplet surface due to the circulation flow inside the relatively large droplet, which is not good for the viability. With suitable droplet spacing and improved single-cell encapsulation efficiency by incorporating a microfluidic flow-focusing device for reduction of droplet size and maintenance of cell viability, the device can be further applied to single cell-based analysis systems.

On the basis of this droplet interval control, we also demonstrated a dynamic temporal control of two distinct droplets using an additional inlet for another sample. As shown in Fig. 6(a), non-dyed (blue) and dyed (orange) droplets were generated at 1st and 2nd T-junctions, respectively. The diameter of each droplet was approximately 59.4 μm. For synchronization of droplets, each droplet was temporally controlled by each control oil flow (e.g., Q_{c1} and Q_{c2}) along the microtunnels and brought together in the confluence channel nearby outlet. Due to the difference in the droplet interval of the two distinct droplets by changing control oil flow rate, the ratio in droplet pairs could be efficiently adjusted. The ratio of droplet pairing (non-dyed: dyed) could be observed in the confluence channel which was dynamically adjusted as 1:2 ($Q_{c1} = 80$ μl/h and $Q_{c2} = 10$ μl/h), 1:1 ($Q_{c1} = 20$ μl/h and $Q_{c2} = 20$ μl/h), and 2:1 ($Q_{c1} = 20$ μl/h and $Q_{c2} = 60$ μl/h), as shown in Figs. 6(b)–6(d). The fixed flow rates of each sample (Q_{r1} and Q_{r2}) and each oil phase (Q_{o1} and Q_{o2}) were 4 and 20 μl/h, respectively. Droplet pairing with various ratios of two distinct droplets would be reproducibly produced by changing the flow rates in each control channel. Also, the entire length of each produced droplet pair would be controlled as a function of flow rate difference between two control oil flows. By adjusting the number of additional inlets including various samples and control channels, the component and sequence of droplet pairs would be controlled. Compared with other droplet pairing methods, the remarkable advantage of this approach is that the interval and pairing ratio of particular droplets can be flexibly and precisely controlled by the control oil flow without any extra operation of droplet-generating flow and integration issues for external fields. The utility of periodic control of droplets provides broad applicability in microfluidic biochemical reactions which require time and volume-dependent reactions. Furthermore, other microfluidic components such as pillar microstructure[21] and built-in electrode[22] can be applied to enhanced coalescence of droplets for achieving advanced combinatorial reactions in a large scale screening applications. Particularly, current platform can be adapted to carry out on-chip serial dilution for measuring rapid enzymatic kinetics, studying protein–protein interactions and performing biological dilution assays. It is anticipated that the proposed on-chip polymerization method combined with a droplet pairing technique will be applicable for paired bead-based analysis.[23]

IV. CONCLUSIONS

In this paper, we have designed and characterized a microfluidic device integrated with simple microbridge structures for the temporal control of aqueous droplets. As the control oil flow rate increased, the droplet interval was increased without any effect on the droplet size or generating pattern. This temporal control of droplets will give an opportunity to achieve precise droplet synchronization. We also validated that the additional control oil flow including calcified oleic acid promoted rapid gelation of alginate beads and collection with sufficient spacing at the outlet. The main drawback of using oleic acid as a continuous phase is that the prolonged exposure to the oleic acid will cause damage to cells due to its acidity and low gas permeability. However, these questions relating to biocompatibility would be settled by including the flushing-out process of oleic acid after the gelation of alginate beads to prevent the viability declining.[24] In this respect, introduction of the pure oil instead of oleic acid as a control flow can be further used to preserve cell viability during the gelling process. The proposed microbridge structures will also play a critical role in performing the on-chip rapid oil exchange. Parallel control of two distinct picoliter droplets for synchronization and production of combinatorial droplet pairs was also demonstrated. It is anticipated that this microfluidic module will support and develop the advanced droplet-based experiments for a wide range of biochemical applications, including biological assay, combinatorial synthesis, and high-throughput screening.

ACKNOWLEDGMENTS

This research was supported by the National Research Laboratory (NRL) Program grant (R0A-2008-000-20109-0) and by the Nano/Bio Science and Technology Program grants (2008-00771) through the National Research Foundation of Korea funded by the Ministry of Education, Science and Technology (MEST). We also acknowledge Chae Yun Bae for technical support and discussion.

[1]S.-Y. Teh, R. Lin, L.-H. Hung, and A. P. Lee, Lab Chip **8**, 198 (2008).
[2]H. Song, D. L. Chen, and R. F. Ismagilov, Angew. Chem. Int. Ed. **45**, 7336 (2006).
[3]E. Um, D.-S. Lee, H.-B. Pyo, and J.-K. Park, Microfluid. Nanofluid. **5**, 541 (2008).
[4]B. Zheng, L. S. Roach, and R. F. Ismagilov, J. Am. Chem. Soc. **125**, 11170 (2003).
[5]M. Prakash and N. Gershenfeld, Science **315**, 832 (2007).
[6]M. Srisa-Art, D.-K. Kang, J. Hong, H. Park, R. J. Leatherbarrow, J. B. Edel, S.-I. Chang, and A. J. deMello, ChemBioChem **10**, 1605 (2009).
[7]R. Tewhey, J. B. Warner, M. Nakano, B. Libby, M. Medkova, P. H. David, S. K. Kotsopoulos, M. L. Samuels, J. B. Hutchison, J. W. Larson, E. J. Topol, M. P. Weiner, O. Harismendy, J. Olson, D. R. Link, and K. A. Frazer, Nat. Biotechnol. **27**, 1025 (2009).
[8]A. Huebner, D. Bratton, G. Whyte, M. Yang, A. J. deMello, C. Abell, and F. Hollfelder, Lab Chip **9**, 692 (2009).
[9]M. He, J. S. Edgar, G. D. M. Jeffries, R. M. Lorenz, J. P. Shelby, and D. T. Chiu, Anal. Chem. **77**, 1539 (2005).
[10]J. J. Agresti, E. Antipov, A. R. Abate, K. Ahn, A. C. Rowat, J.-C. Baret, M. Marquez, A. M. Klibanov, A. D. Griffiths, and D. A. Weitz, Proc. Natl. Acad. Sci. U.S.A. **107**, 4004 (2010).
[11]L.-H. Hung, K. M. Choi, W.-Y. Tseng, Y.-C. Tan, K. J. Shea, and A. P. Lee, Lab Chip **6**, 174 (2006).
[12]D. R. Link, E. Grasland-Mongrain, A. Duri, F. Sarrazin, Z. Cheng, G. Cristobal, M. Marquez, and D. A. Weitz, Angew. Chem. Int. Ed. **45**, 2556 (2006).
[13]K. Ahn, J. Agresti, H. Chong, M. Marquez, and D. A. Weitz, Appl. Phys. Lett. **88**, 264105 (2006).
[14]E. Um and J.-K. Park, Lab Chip **9**, 207 (2009).
[15]S. Zeng, B. Li, X. Su, J. Qin, and B. Lin, Lab Chip **9**, 1340 (2009).
[16]L. Frenz, J. Blouwolff, A. D. Griffiths, and J.-C. Baret, Langmuir **24**, 12073 (2008).
[17]C.-W. Li, R. Chen, and M. Yang, Lab Chip **7**, 1371 (2007).
[18]T. Thorsen, R. W. Roberts, F. H. Arnold, and S. R. Quake, Phys. Rev. Lett. **86**, 4163 (2001).
[19]G. A. Truskey, F. Yuan, and D. F. Katz, *Transport Phenomena in Biological Systems* (Prentice Hall, New Jersey, 2004).
[20]V. Labrot, M. Schindler, P. Guillot, A. Colin, and M. Joanicot, Biomicrofluidics **3**, 012804 (2009).
[21]X. Niu, S. Gulati, J. B. Edel, and A. J. deMello, Lab Chip **8**, 1837 (2008).
[22]X. Niu, F. Gielen, A. J. deMello, and J. B. Edel, Anal. Chem. **81**, 7321 (2009).
[23]T. Teshima, H. Ishihara, K. Iwai, A. Adachi, and S. Takeuchi, Lab Chip **10**, 2443 (2010).
[24]C. Kim, K. S. Lee, Y. E. Kim, K.-J. Lee, S. H. Lee, T. S. Kim, and J. Y. Kang, Lab Chip **9**, 1294 (2009).